Analyst

RSC Publishing

PAPER

View Article Online
View Journal | View Issue

Cite this: *Analyst*, 2013, **138**, 4599

Quantification of tumor necrosis factor-α and matrix metalloproteinases-3 in synovial fluid by a fiber-optic particle plasmon resonance sensor

Yi-Ching Huang,[ab] Chang-Yue Chiang,[ab] Cheng-Hen Li,[a] Ting-Chou Chang,[a] Chung-Sheng Chiang,[b] Lai-Kwan Chau,*[ab] Kuo-Wei Huang,[b] Chin-Wei Wu,[a] Shau-Chun Wang[ab] and Shaw-Ruey Lyu*[cd]

Received 5th February 2013
Accepted 14th May 2013

DOI: 10.1039/c3an00276d

www.rsc.org/analyst

The availability of techniques for sensitive detection of early stage osteoarthritis is critical for improving patient health. This study illustrates the feasibility of a fiber-optic particle plasmon resonance (FOPPR) sensor with gold nanoparticles on the unclad region of optical fiber probes for analysis of osteoarthritis biomarkers, tumor necrosis factor-α (TNF-α) and matrix metalloproteinases-3 (MMP-3). Results show that the sensor can achieve a refractive index resolution of 5.18×10^{-7} RIU and limits of detection for TNF-α and MMP-3 as low as 8.22 pg ml^{-1} (0.48 pM) and 34.3 pg ml^{-1} (1.56 pM), respectively. Additionally, the FOPPR sensor shows a good correlation in determining TNF-α and MMP-3 in synovial fluid with the clinically accepted enzyme-linked immunosorbent assay (ELISA) method. Finally, given the FOPPR sensor's nature of being low-cost, label-free, highly sensitive, real-time, simple-to-operate, the FOPPR sensor could offer potential to monitor biomarkers of various diseases, and provide an ideal technical tool for point-of-care diagnostics.

Introduction

Detection of biomarkers is critical in understanding patients' health status. A variety of technologies have been developed for biomarker detection, such as enzyme-linked immunosorbent assay (ELISA), real-time polymerase chain reaction, quartz crystal microbalance, mass spectrometry, surface plasmon resonance, electrochemical methods, *etc.* Although some of these assay techniques can provide exceptional sensitivity or high selectivity in some cases, they have some disadvantages, such as being time-consuming as well as laborious, having poor precision, expensive, or must be performed by skilled personnel only. Such disadvantages limit the development of rapid, easy to use and low-cost detection systems suitable for implementation at the point-of-care (POC).

Osteoarthritis (OA) is a chronic disability and systemic inflammatory disease of the joints, also known as degenerative joint disease. It can arise in any synovial joint in the body, but is most common in the hands, feet, spine, and large weight-bearing joints, such as the hips and knees.[1,2] OA is characterized pathologically by progressive articular cartilage destruction and loss, new bone formation at the joint margins, changes in the subchondral bone, varying degrees of synovitis and thickening of the joint capsule.[3,4] These pathology changes result in a range of symptoms, including pain, inflammation, joint enlargement, swelling and joint instability or buckling. Joint pain, worsened by weight-bearing activity, is the most prominent symptom of OA and has a significant impact on the function and quality of life of people with OA.[5] Early aggressive therapy is now widely advocated in the hope of improving the long-term outcome for patients. The need for reliable early predictors of the course of the disease is therefore increasing. Although the mechanisms of inflammation in OA are uncertain, the prevailing theory is that cartilage degradation leads to the release of cytokines, matrix metalloproteinases, and other proinflammatory mediators into the joint,[3,6–9] in which, TNF-α and MMP-3 are believed to play important roles in the pathogenesis and progression of the OA knee.[8,9] TNF-α is a proinflammatory cytokine and appears to be responsible for the extent of synovitis,[8,10] whereas MMP-3 is induced by inflammatory cytokines such as TNF-α and interleukin-1β.[4,9] The release of these mediators triggers a cycle of self-propagation whereby more inflammatory mediators are released from synovial cells and also from activated leucocytes and macrophages that are recruited to the joint.[6] This inflammatory cascade may exacerbate joint damage and destruction in OA, including both elevation of cartilage catabolism and suppression of cartilage anabolism, and also activates and sensitizes nerves in

[a]*Department of Chemistry and Biochemistry, National Chung Cheng University, Chiayi, 621, Taiwan. E-mail: chelkc@ccu.edu.tw; Fax: +886 5 2721040; Tel: +886 5 2720411 ext. 66411*

[b]*Center for Nano Bio-Detection, AIM-HI, National Chung Cheng University, Chiayi, 621, Taiwan*

[c]*Joint Center, Buddhist Dalin Tzu Chi General Hospital, Chiayi, 622, Taiwan. E-mail: srlyu@seed.net.tw; Tel: +886 5 2648000 ext. 5901*

[d]*School of Medicine, Tzu Chi University, Hualien, 970, Taiwan*

the synovial tissue, leading to increased pain.[3,11,12] Accordingly, the measurement of these disease biomarkers has become a critical indicator of normal and disease states.

Recently, particle plasmon resonance (PPR) methods, also known as localized surface plasmon resonance (LSPR) methods, have been widely reported for the measurement of chemical and biochemical species, because of the extremely sensitive nature of their electron-rich surfaces to the surrounding environment.[13–18] Particle plasmons are charge density collective oscillation confined to metallic nanoparticles.[19,20] When the incident photon frequency is resonant with the collective oscillation of the conduction electron of the nanoparticle, a peak in the extinction spectrum of the nanoparticle is manifested. In addition, the PPR spectral position and intensity depend on the size, shape, composition, and dielectric environment of the surrounding medium.[21–23] For biosensor applications, gold nanoparticles (AuNPs) are particularly attractive because of their chemical stability and convenient spectral window in the visible region. As the binding of an analyte to the nanoparticle surface will change the local refractive index (RI) surrounding these particles, an increase of the plasmon absorbance and a shift in the PPR wavelength will result. In other words, the nanoparticle acts as a reporter chromophore and its interaction with an analyte will result in a large increase of the absorption coefficient of the nanoparticle,[24] accounting for the high sensitivity of the PPR biosensing methods.[24–26] Furthermore, unlike the SPR system, the PPR biosensor system employs a simple optical extinction measurement. Despite the undisputed advantages of the PPR assays, the issue of the low absorbance of a nanoparticle submonolayer needs to be solved to enhance the sensitivity of detection.[14]

To overcome the issue of low absorption, we have developed a label-free and real-time fiber-optic particle plasmon resonance (FOPPR) sensor, which is based on a gold nanoparticle-modified optical fiber.[22] This sensor utilizes the evanescent wave *via* the multiple total internal reflection (TIR) scheme to increase the absorbance of a submonolayer of AuNPs on the fiber core and significantly enhance the signal-to-noise (*S*/*N*) ratio achieved by the AuNP submonolayer sensing structure.

Over the past years, the FOPPR sensor has been used for the detection of various chemical and biological compounds related to areas such as environmental protection (*e.g.* heavy metal ion), medical diagnostics (*e.g.* antinuclear antibodies and cytokines), food safety monitoring (*e.g.* staphylococcus enterotoxin B, SEB), and agricultural detection (*e.g.* orchid virus).[22,23,25–28] According to these results, the FOPPR sensor has been experimentally demonstrated with linear calibration curves, good reproducibility, and low detection limit in the analysis of chemical and biochemical samples.

This work demonstrates the application of the FOPPR sensor to label-free and real-time detection of representative osteoarthritis concerned biomarkers, TNF-α and MMP-3 in synovial fluid samples as a rapid and user-friendly alternative to conventional techniques. A comparison of its performance with enzyme-linked immunosorbent assay (ELISA), the gold standard in immunoassay, will also be discussed. The FOPPR sensor has high sensitivity, wide linear range, and good selectivity, which may be extendable to the detection of other protein molecules to fit a variety of applications.

Experimental

Materials and reagents

Hydrogen tetrachloroaurate trihydrate ($HAuCl_4$), 11-mercaptoundecanoic acid (MUA; ≥95%), 6-mercapto-1-hexanol (MCH; ≥97%), and bovine serum albumin (BSA, molecular mass = 67 kDa) were purchased from Sigma-Aldrich. Recombinant human matrix metalloproteinase-3 (MMP-3, molecular mass = 22 kDa), monoclonal anti-human MMP-3 (anti-MMP-3), and recombinant human interferon gamma (IFN-γ, molecular mass = 17 kDa) were obtained from ProSpec (Rehovot, Israel). Recombinant human tumor necrosis factor alpha (TNF-α, molecular mass = 17 kDa) and monoclonal anti-human tumor necrosis factor alpha (anti-TNF-α) were purchased from R&D systems. Cetyltrimethylammonium bromide (CTAB), *N*-hydroxy-succinimide (NHS), 1-ethyl-3-(3-dimethylaminopropyl)-carbodiimine hydrochloride (EDC), and (3-mercaptopropyl)-trimethoxysilane (MPTMS, 98%) were obtained from Fluka. Sodium borohydride ($NaBH_4$) was purchased from Lancaster. All the aqueous solutions were made up by purified water, which was deionized by a Millipore Milli-Q water purification system (Millipore) with a specific resistance of 18.2 MΩ. Multimode plastic-clad silica optical fiber was purchased from Newport (model F-MBC) with core and cladding diameters of 400 and 430 μm, respectively. Removal of optical fiber coating and cladding was done by a CO_2 laser engraving process.

Microchip fabrication

The sensor chip was composed of two cyclic olefin copolymer (COC) plates, a cover and a bottom plate, with dimensions of 2.5 cm (width) × 5 cm (length) × 0.2 cm (thickness) and fabricated by an injection molding machine. The bottom plate contained a microchannel with a depth of 800 μm and a width of 800 μm. An inlet and an outlet for sample introduction were connected to two small access holes and mechanically bored into the microchannel. The total length of the optical fiber was 8 cm and the sensing zone (the unclad portion) in the middle segment was 2 cm. The cover and the bottom plates were glued by 3M sticker to form the chip. Teflon tubing was then attached to the chip at inlet and outlet channels.

Biosensing system

A schematic of our biosensing system is shown in Fig. 1A, which consists of a light-emitting diode (LED, model IF-E93, Industrial Fiber Optic, Inc.) with a peak wavelength of 530 nm, a LED driver circuit to drive the LED with 1 kHz frequency modulation (with auto-voltage control, home-made), a FOPPR sensor chip, a detection photodiode (S1336-18BK, Hamamatsu), a photoreceiver amplification circuit (photodiode current/voltage converter and amplifier), a feedback module (home-made), and a lock-in module (USB-9234 and LabVIEW software, National Instrument). The feedback module, which comprises a reference photodiode, a photoreceiver amplification circuit, a

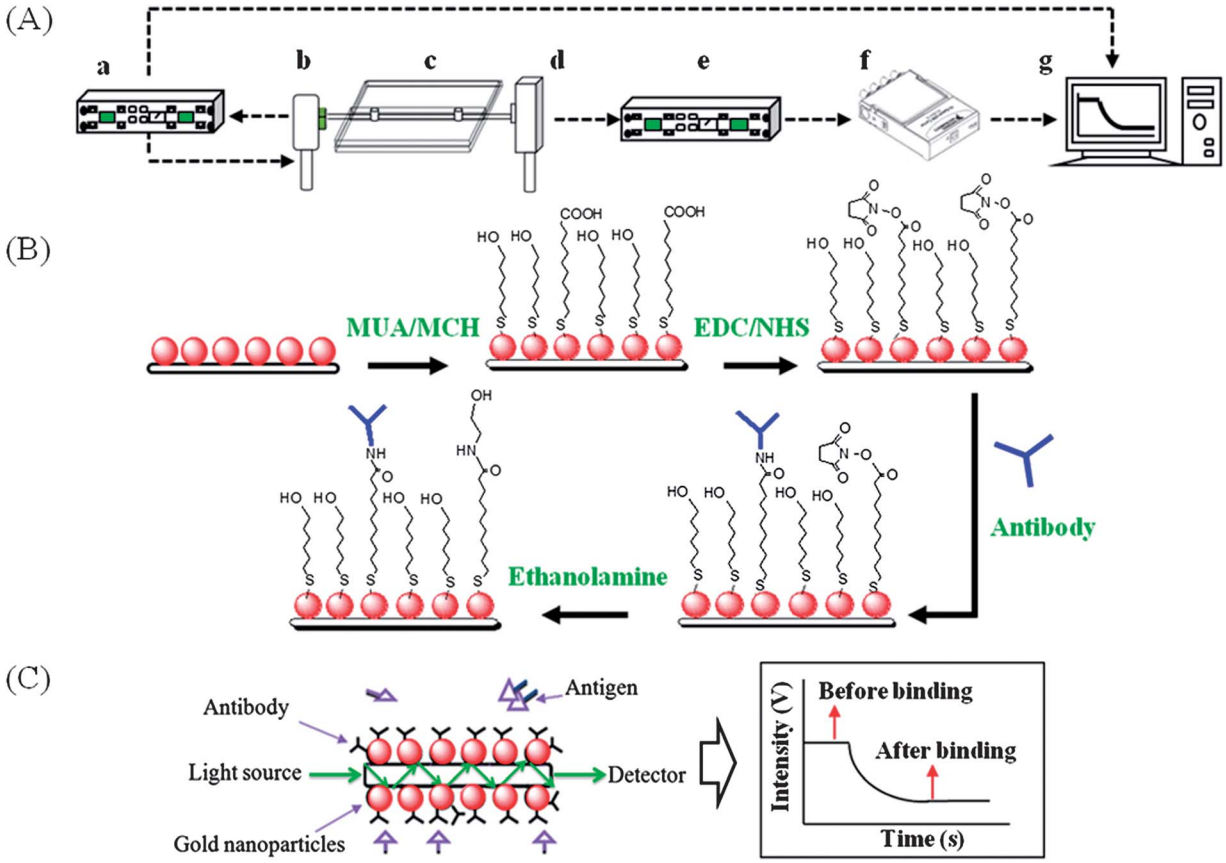

Fig. 1 (A) Schematic representation of the experimental setup used for the fiber-optic particle plasmon resonance (FOPPR) sensing system. The setup consists of: (a) LED driver circuit and feedback module; (b) light-emitting diode; (c) FOPPR sensor chip; (d) photodiode; (e) photoreceiver amplification circuit; (f) lock-in module; (g) computer. (B) Schematic of the steps involved in the fabrication of the sensor fiber. The various components are not drawn to scale. (C) Biomolecular binding on the functionalized AuNP surface of the fiber sensor results in a decrease in light intensity exiting the optical fiber.

demodulation circuit, and a feedback circuit, is designed to reduce the noise and measurement-to-measurement variation. Details of the feedback module will be reported elsewhere.

Antibody immobilization

Spherical Au nanoparticles (AuNPs) were prepared according to the procedures as previously described.[22] The AuNPs were then self-assembled on the unclad portion of an optical fiber. To functionalize the surface of AuNPs with anti-TNF-α or anti-MMP-3 (shown in Fig. 1B), a mixed self-assembled monolayer (SAM) of MCH and MUA is formed by immersing the AuNP-modified optical fiber into an ethanol solution of MUA (2 mM) and MCH (2 mM) in a volume ratio of 1 : 4 overnight at room temperature, then rinsed with ethanol and N_2-dried. Subsequently, the mixed SAM was modified by activation of the –COOH group into NHS ester with EDC and NHS by immersing into an aqueous solution of EDC (0.1 M) and NHS (0.1 M) for 2 h at 4 °C.

Then anti-TNF-α or anti-MMP-3 was immobilized on the surface by immersing in a solution of anti-TNF-α or anti-MMP-3 with a concentration of 100 μg ml^{-1} overnight at 4 °C. The nonspecifically bound antibodies were washed away and the nonreacted sites on the monolayer were deactivated by rinsing the monolayer with an aqueous solution of 1 M ethanolamine with a pH of 8.5 for 30 min. Finally, the antibody-immobilized surface was rinsed thoroughly with phosphate buffer saline (PBS) solution (pH 7.4, 150 mM NaCl, 4 mM KCl, 8.1 mM Na_2HPO_4, and 1.47 mM KH_2PO_4).

Preparation of standards and samples

Stock standard solutions were prepared in PBS, and were stored in a freezer at −20 °C. The standard solutions of TNF-α and MMP-3 were prepared in a concentration range of 0.019 to 1250 ng ml^{-1} and 0.05 to 50 ng ml^{-1}, respectively, by serial dilution of the stock solution and stored at 4 °C until use. This study has been evaluated and approved by the ethics committee of Tzu Chi hospital. The synovial fluids of the knee joints collected from patients suffering from OA were provided by Tzu-Chi hospital. The samples were stored at −80 °C until use. Each sample was diluted by PBS buffer and then a centrifugal filter device (Amicon Ultra-4, Millipore) was used to remove blood cells and proteins by three stages of centrifuging at 3600 rpm for 15 min.

Procedure for ELISA

The sandwich ELISA method was used. Human MMP-3 immunoassays were purchased from Bioo Scientific; human

TNF-α immunoassay was purchased from R&D systems. All operations were according to the instructions. The absorbance was read at 450 nm using a Bio-Rad model 680 Microplate reader.

Statistical analysis

Regression analysis was used to determine the correlation between the FOPPR and ELISA methods. The analysis was performed using the InStat version 3.0 software (GraphPad Software, Inc.) and M_{ED} C_{ALC}® for windows version 11.4.2.0.

Results and discussion

Principle

The principle of the sensing technique relies on the penetration of the evanescent wave in the absorbing medium outside the fiber core. Since light propagates in the optical fiber by virtue of multiple TIRs, the evanescent field on the fiber core surface excites the PPRs of immobilized AuNPs and thus the light transmitted through the optical fiber is attenuated by interaction with AuNPs.[27,30] As the attenuation is enhanced by multiple TIRs, the low absorbance of a nanoparticle submonolayer can be significantly enhanced, as illustrated in Fig. 1C.[22,27] The absorption coefficient of the AuNP layer increases when the AuNP's surrounding RI increases.[26] Hence, the increase of local RI on the AuNP surface after molecular binding can be revealed by a decrease of transmitted light intensity through the optical fiber. In this study, the quantitative analyses of evanescent wave absorption measurements of the FOPPR sensor are performed by comparing the collected optical signal of a sensor immersed in an analyte solution (I_S) to the intensity of the sensor immersed in a blank solution (I_R). The sensor response is defined as $(I_R - I_S)/I_R = \Delta I/I_R$.

Two parameters, refractive index sensitivity (RIS) and refractive index resolution (RIR), are used to characterize the sensor performances. The RIS to RI change is the slope of the plot of the sensor response *versus* RI.[23] The RIR is defined as the minimum change in the refractive index unit (RIU) that can be resolved by the sensor, where the noise is taken as the standard deviation of the sensor response for 10 repetitive measurements of a blank.[29] In this study, an estimate of the root-mean-square noise of the sensor in a blank is 0.015 mV and this corresponds to a relative error of 0.0045% per 1000 s when normalized to I_R. As shown in Fig. 2, using sucrose solutions of various refractive indices, the signal intensity shows a step-down trend with the step-wise increase of RI and the plot of $\Delta I/I_R$ *versus* RI shows a good linear relationship (correlation coefficient, $R = 0.9994$). The RIS of the sensor form is calculated to be 5.18×10^{-7} RIU, which is better than or comparable to many refractive-index-based sensors.[31] In addition, seven repetitive measurements of the above series of sucrose solutions were used to estimate the precision of the present sensing platform. From these measurements, the coefficient of variation (CV) was found to be 1.25–5.65%, indicating that the present FOPPR sensor offers excellent reproducibility and stability.

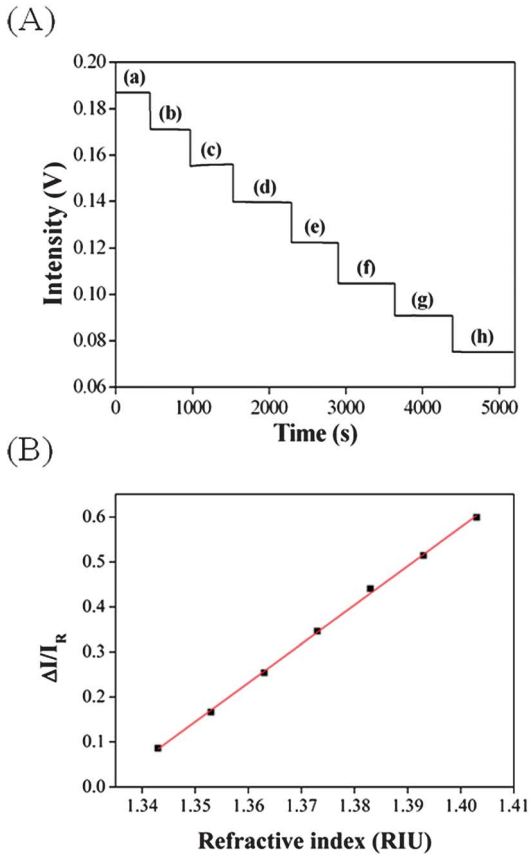

Fig. 2 (A) Temporal response of the FOPPR sensor signal with serial injection of samples with refractive index of (a) 1.333, (b) 1.343, (c) 1.353, (d) 1.363, (e) 1.373, (f) 1.383, (g) 1.393, and (h) 1.403. (B) Dependency of the FOPPR sensor signal expressed as $\Delta I/I_R$ on the RI of the surrounding medium of AuNPs.

Nonspecific adsorption test

For biosensor applications in real samples, nonspecific adsorption is an important issue, especially for biosensors based on detection of refractive index change near the biosensor surface. Typically, this problem can be minimized by the use of molecular films with hydroxyl (–OH) or glycol moieties on the gold surface to cover the space besides the probe molecules. This strategy has been widely used by many research groups[32,33] and our previous experience shows that such an approach is effective.[18,34,35] We extended this strategy to this study, and the nonspecific adsorption tests were carried out with a high concentration of BSA (10^{-4} g ml^{-1}) or IFN-γ (10^{-4} g ml^{-1}) in PBS buffer. As shown in Fig. 3, the sensor response in the presence of BSA or IFN-γ was indistinguishable from the background, indicating that there is no nonspecific binding to the optical fiber probes. Furthermore, irrelevant antibodies such as anti-IL-1β and anti-IFN-γ have been used to test the specificity of TNF-α and MMP-3 towards these irrelevant antibodies and no nonspecific binding was found.

Calibration curves by the FOPPR sensor and ELISA

As the above results are encouraging, we used the FOPPR sensing platform to construct calibration curves for TNF-α and

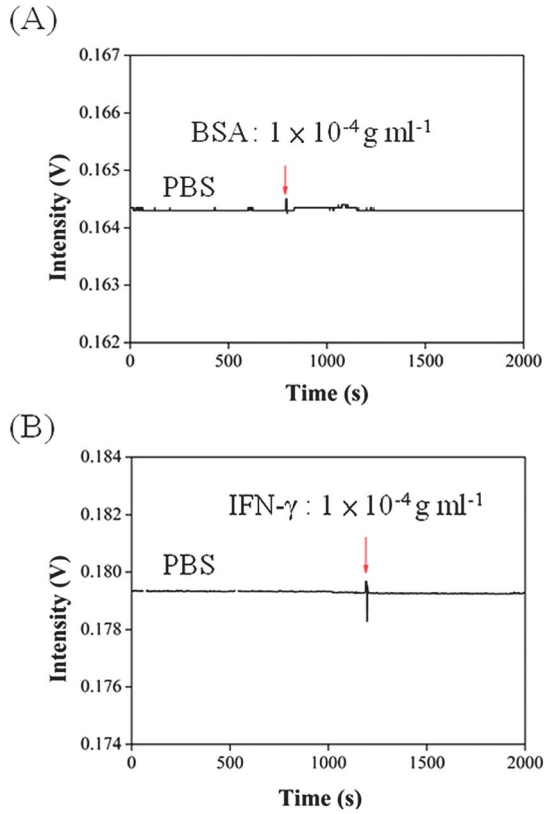

Fig. 3 Nonspecific adsorption tests: (A) the response of the optical fiber probe in the presence of 1.0×10^{-4} g ml^{-1} BSA (67 kDa); (B) the response of the optical fiber probe in the presence of 1.0×10^{-6} g ml^{-1} IFN-γ (17 kDa).

MMP-3 in PBS buffer. The standards of human TNF-α and MMP-3 were diluted serially with PBS buffer ranging between 0.019 ng ml^{-1} and 1250 ng ml^{-1} to construct calibration curves for the FOPPR sensor and ELISA. Fig. 4 shows an example of the serial sensor responses from an optical fiber probe functionalized with anti-TNF-α upon injection of a PBS buffer solution and then sequential injection of TNF-α up to a final concentration of 1250 ng ml^{-1}. The calibration curves as shown in Fig. 5 demonstrate that the FOPPR sensor is outstanding to detect very low concentrations and they show a good linear relationship (R = 0.9983 for TNF-α and R = 0.9996 for MMP-3). The limits of detection (LOD, with S/N ratio = 3 : 1) of the sensor for TNF-α and MMP-3 are calculated to be 8.2 pg ml^{-1} (0.48 pM) and 34 pg ml^{-1} (1.6 pM), respectively. Besides, the linear dynamic ranges (LDRs) of the FOPPR sensor (0.019 to 1250 ng ml^{-1} for TNF-α; 0.05 to 50 ng ml^{-1} for MMP-3) are wider in comparison with ELISA while the LODs are slightly better than those by ELISA (18 pg ml^{-1} (1.06 pM) for TNF-α and 74 pg ml^{-1} (3.22 pM) for MMP-3). A comparison of the analytical performance by both methods is summarized in Table 1.

Furthermore, the LODs achieved by the FOPPR sensor are superior to those achieved by the SPR sensors (74 pM for TNF-α by the fiber-optic SPR sensor and 140 pM for MMP-3 by the SPR sensor).[36,37] Moreover, the limits of quantification (LOQ, with S/N ratio = 10 : 1) of the sensor for TNF-α and MMP-3 are calculated to be 13 pg ml^{-1} (0.75 pM) and 71 pg ml^{-1} (3.2 pM),

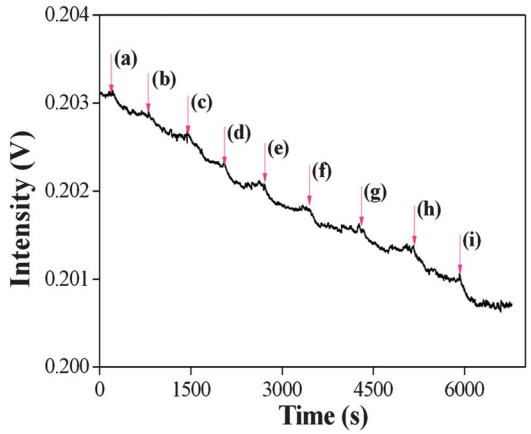

Fig. 4 Real-time detection of the serially diluted TNF-α standard solutions: (a) 1.91×10^{-11} g ml^{-1}, (b) 7.63×10^{-11} g ml^{-1}, (c) 3.05×10^{-10} g ml^{-1}, (d) 1.22×10^{-9} g ml^{-1}, (e) 4.88×10^{-9} g ml^{-1}, (f) 1.95×10^{-8} g ml^{-1}, (g) 7.81×10^{-8} g ml^{-1}, (h) 3.13×10^{-7} g ml^{-1}, and (i) 1.25×10^{-6} g ml^{-1}.

respectively. Furthermore, the response time (time to reach 90% of the equilibrium signal level) as shown in Fig. 4 is about 290 s and a steady signal can be observed in <10 min. Such an analysis time is much shorter than the time required (~6 h) by ELISA to take the final reading.

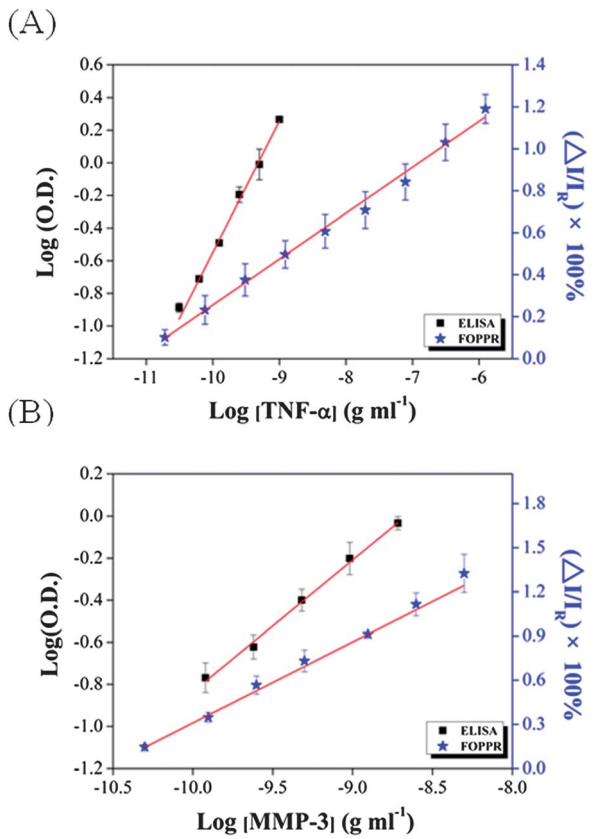

Fig. 5 (A) Calibration graphs for TNF-α by (a) ELISA and (b) anti-TNF-α-conjugated FOPPR sensor (n = 3). (B) Calibration graphs for MMP-3 by (a) ELISA and (b) anti-MMP-3-conjugated FOPPR sensor (n = 3).

Table 1 Comparison of the analytical performance by the FOPPR sensor and the ELISA methods for detection of TNF-α and MMP-3

Method	Analyte	LDR (ng ml^{-1})	Analysis time	LOD (pg ml^{-1})
FOPPR	TNF-α	0.019–1250	<10 min	8.2
	MMP-3	0.05–50	<10 min	34
ELISA	TNF-α	0.062–0.03	~6 h	18
	MMP-3	0.06–1.92	~6 h	74

Evaluation of binding affinity and kinetics

The availability of real-time FOPPR kinetic data may provide insight into the nature of protein–protein interactions and thus the mechanism of the binding events. Using an approach as previously described[38] to evaluate the kinetic rate constants and binding affinity of anti-TNF-α binding with TNF-α, the linear fits yield the association rate constant (k_a) and dissociation rate constant (k_d) of 3.5×10^7 M^{-1} s^{-1} and 4.82×10^{-2} s^{-1}, respectively. Then we use the k_a and k_d values to calculate the affinity constant, K_f, (where $K_f = k_a/k_d$), and yields $(7.45 \pm 0.64) \times 10^8$ M^{-1} ($n = 3$). The average K_f value is in good agreement with previously reported values determined by fiber-optic SPR (8.2×10^8 M^{-1}) and conventional SPR (1.3×10^8 M^{-1}).[36,39] Similarly, the k_a and k_d of anti-MMP-3 binding with MMP-3 are estimated to be 1.62×10^6 M^{-1} s^{-1} and 1.67×10^{-2} s^{-1}, respectively, while the K_f is calculated to be $(9.53 \pm 0.12) \times 10^7$ M^{-1} ($n = 3$).

Real clinical sample determination

Twelve samples of synovial fluids from OA patients were collected from the Buddhist Dalin Tzu Chi General Hospital. Synovial fluid samples were diluted using PBS buffer and filtered by centrifugation to minimize the matrix effect and to keep the refractive index of the treated sample to be similar to those of standards. Upon dilution of several samples with various dilution factors, we found that a dilution of 25-fold was optimal.[26] As determined by the FOPPR biosensor and the ELISA method, the TNF-α concentration and the MMP-3 concentration in the synovial fluids of the OA patients fall in the range of 2–7 pM and 57–675 pM, respectively, as shown in Table 2. What deserves to be mentioned is that the proinflammatory cytokine TNF-α is believed to be involved in the initiation and progression of OA while MMP-3 is suggested to contribute to cartilage degradation.[40] The concentrations of TNF-α and MMP-3 in the synovial fluid may reflect various degrees of OA progression. Thus, multiplexed detection of TNF-α and MMP-3 is important not only for the treatment in the early stage but also for the investigation of pathogenesis. The FOPPR biosensor may provide a possibility for real-time and *in situ* detection of localized cytokines and cartilage degradation enzymes in different compartments of OA joints.

Comparative analysis of synovial fluid samples on TNF-α and MMP-3 levels obtained by the FOPPR sensor and ELISA method

The accuracy of the FOPPR sensor for the determination of TNF-α and MMP-3 was examined by comparing the FOPPR sensor responses in the synovial fluid samples obtained from 12 OA patients with those of the ELISA method results. Statistical analysis of the two groups of results was performed by linear

Table 2 The TNF-α and MMP-3 concentrations measured in synovial fluid samples from 12 OA patients ($n = 3$)

Protein concentration (mean ± SD) in synovial fluid samples by FO-PPR and ELISA (pM)				
	TNF-α		MMP-3	
Sample	FOPPR	ELISA	FOPPR	ELISA
No. 1	2.1 ± 0.4	1.6 ± 0.4	172 ± 38	186 ± 11
No. 2	4.9 ± 0.8	4.9 ± 0.5	183 ± 10	175 ± 5
No. 3	3.8 ± 0.8	3.6 ± 0.9	518 ± 23	675 ± 16
No. 4	6.9 ± 0.5	6.6 ± 0.8	123 ± 11	126 ± 25
No. 5	4.0 ± 0.4	4.3 ± 0.5	101 ± 18	87.6 ± 5.2
No. 6	2.6 ± 0.4	2.6 ± 0.6	113 ± 17	139 ± 6
No. 7	2.8 ± 1.1	2.4 ± 1.2	147 ± 17	178 ± 8
No. 8	6.3 ± 1.0	6.4 ± 0.5	121 ± 15	178 ± 9
No. 9	4.6 ± 0.3	4.7 ± 0.3	56.9 ± 3.7	Nd[a]
No.10	4.2 ± 0.2	4.1 ± 0.4	81.8 ± 3.4	128 ± 3
No.11	2.5 ± 0.5	2.4 ± 0.5	79.6 ± 8.5	118 ± 2
No.12	2.0 ± 0.2	1.8 ± 0.5	381 ± 37	418 ± 23

[a] Nd = not detected.

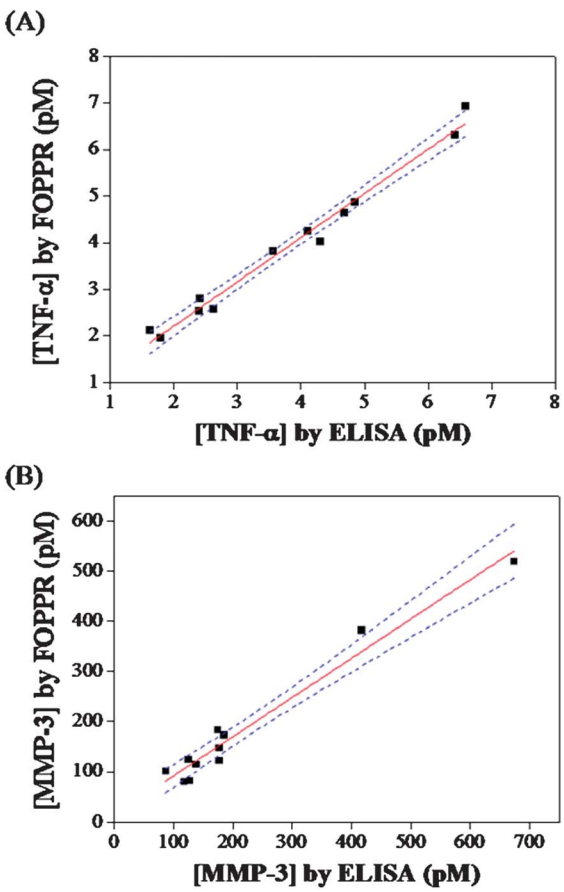

Fig. 6 Graphs displaying the correlation between FOPPR sensor and ELISA results for detection of (A) TNF-α and (B) MMP-3 in synovial fluid samples. The dashed line shows the 95% confidence interval for prediction with the linear regression model.

correlation analysis and the p value was <0.0001 at the 95% level of significance, indicating that the results of each sample by both methods are in agreement with each other. Since ordinary least-squares regression analysis presumes that the measurements for one of the methods are without random error and the analytical standard deviation for the other method is constant throughout the measurement range but both assumptions are rarely fulfilled, the Deming linear regression which takes into account random errors in both methods was employed to verify the methods comparison data.[41] Results confirm that the p value was <0.0001 at the 95% level of significance. It should be noted that the MMP-3 concentration in sample 9 (Table 2) is too low to be detected by ELISA but is detectable by the FOPPR sensor. Additionally, the 12 pairs of data for TNF-α and 11 pairs of data for MMP-3 (exclude sample 9 in Table 1) by these two methods showed a good correlation coefficient of 0.9914 and 0.9824, respectively, from the linear regression analysis, as shown in Fig. 6, and 0.9918 and 0.9824, respectively, from the Deming regression analysis. These results suggest that the label-free and real-time detection capabilities of the FOPPR sensor for protein analysis can serve as a good immunoassay alternative to the laborious and time-consuming ELISA method.

Conclusions

In summary, the FOPPR sensor provides a label-free, real-time, and high sensitivity detection platform for biomolecular detection. Since the principle of FOPPR measurements is based on absorption spectroscopy, normalization of the sensor response by $\Delta I/I_R$ alleviates the need for precise optical alignment. Such a normalization procedure also yields reasonably good chip-to-chip measurement reproducibility. Moreover, when a reasonably stable biorecognition molecule is used, regeneration and hence reuse of the sensor surface have been demonstrated.[29] The limits of detection of the sensor for TNF-α and MMP-3 are 8.2 pg ml^{-1} (0.48 pM) and 34 pg ml^{-1} (1.6 pM), respectively. As TNF-α has emerged as one of the mediators that interferes with both antiproliferative and tumorigenic effects and the concentration of TNF-α in biological fluids is very low (~20 pg ml^{-1} in a healthy person),[42] this sensor may provide the sensitivity for early detection of cancer.

Although the results reported here are encouraging, much remains to be done in order to develop the FOPPR sensor for practical applications. Common to refractive-index-based biosensors, the high refractive index sensitivity of a sensor also means that the measurement is highly sensitive to the refractive index variation in the medium of real samples. As a result, dilution of real samples is required to avoid the change in the refractive index of the sample medium. The dilution procedure not only compromises the sensitivity but also lengthens the procedure. Therefore, we have developed a self-referencing multichannel FOPPR biosensing platform. This platform will not only compensate for changes in the bulk refractive index of the sample medium but also provide simultaneous analysis of multiple samples in a parallel format, while it requires a significant shorter analysis time than ELISA.

Finally, the principle of the FOPPR described in this study can be generalized to other biomarkers of OA or cancer by changing the specific antibody, producing new immunosensors which may have significant application in clinical sample testing. Challenges remain in improving the sensitivity of clinical immunoassays to meet the increasing demand for early disease diagnosis. The high-sensitivity and cost-effectiveness of the FOPPR biosensor may be able to play a role here. Moreover, POC is receiving increasing attention nowadays, but ideal POC devices are being challenged by small sample volumes of complex biological media with femtomolar to millimolar concentrations of analytes.[43] The simple and low-cost optical setup of this sensor potentially is easy to be miniaturized and hence can be implemented at the POC.

Acknowledgements

Support for this research from the Buddhist Dalin Tzu Chi General Hospital through grant number 98-1-2 and the National Science Council (Taiwan) through grant number NSC95-3114-P-194-001-MY3 is acknowledged.

Notes and references

1 X. Ayral, E. H. Pickering, T. G. Woodworth, N. Mackillop and M. Dougados, *Osteoarthritis Cartilage*, 2005, **13**, 361.
2 E. Hedbom and H. J. Häuselmann, *Cell. Mol. Life Sci.*, 2002, **59**, 45.
3 M. Daheshia and J. Q. Yao, *J. Rheumatol.*, 2008, **35**, 2306.
4 H.-S. Wang, P.-Y. Kuo, C.-C. Yang and S.-R. Lyu, *Histopathology*, 2011, **58**, 593.
5 M. Nunez, E. Nunez, S. Sastre, J. L. Del-Val, J. M. Segur and F. Macule, *Orthopedics*, 2008, **31**, 753.
6 A. Shibakawa, H. Aoki, K. Masuko-Hongo, T. Kato, M. Tanaka, K. Nishioka and H. Nakamura, *Osteoarthritis Cartilage*, 2003, **11**, 133.
7 G. H. Yuan, M. Tanaka, K. Masuko-Hongo, A. Shibakawa, T. Kato, K. Nishioka and H. Nakamura, *Osteoarthritis Cartilage*, 2004, **12**, 38.
8 M. Attur, J. Samuels, S. Krasnokutsky and S. B. Abramson, *Best Pract. Res., Clin. Rheumatol.*, 2010, **24**, 71.
9 J. Martel-Pelletier, D. J. Welsch and J.-P. Pelletier, *Best Pract. Res., Clin. Rheumatol.*, 2001, **15**, 805.
10 M. Niedermeier, T. Pap and A. Korb, *Best Pract. Res., Clin. Rheumatol.*, 2010, **24**, 527.
11 M. J. Benito, D. J. Veale, O. FitzGerald, W. B. van den Berg and B. Bresnihan, *Ann. Rheum. Dis.*, 2005, **64**, 1263.
12 W. van den Berg, *Arthritis Res.*, 2001, **3**, 18.
13 N. Nath and A. Chilkoti, *Anal. Chem.*, 2002, **74**, 504.
14 N. Nath and A. Chilkoti, *Anal. Chem.*, 2004, **76**, 5370.
15 F. Frederix, J.-M. Friedt, K.-H. Choi, W. Laureyn, A. Campitelli, D. Mondelaers, G. Maes and G. Borghs, *Anal. Chem.*, 2003, **75**, 6894.
16 A. B. Dahlin, J. O. Tegenfeldt and F. Höök, *Anal. Chem.*, 2006, **78**, 4416.
17 K. Mitsui, Y. Handa and K. Kajikawa, *Appl. Phys. Lett.*, 2004, **85**, 4231.

18 V. V. R. Sai, T. Kundu and S. Mukherji, *Biosens. Bioelectron.*, 2009, **24**, 2804.
19 K. A. Willets and R. P. Van Duyne, *Annu. Rev. Phys. Chem.*, 2007, **58**, 267.
20 M. E. Stewart, C. R. Anderton, L. B. Thompson, J. Maria, S. K. Gray, J. A. Rogers and R. G. Nuzzo, *Chem. Rev.*, 2008, **108**, 494.
21 E. Hutter and J. H. Fendler, *Adv. Mater.*, 2004, **16**, 1685.
22 S.-F. Cheng and L.-K. Chau, *Anal. Chem.*, 2002, **75**, 16.
23 K.-W. Huang, C.-W. Hsieh, H.-C. Kan, M.-L. Hsieh, S. Hsieh, L.-K. Chau, T.-E. Cheng and W.-T. Lin, *Sens. Actuators, B*, 2012, **163**, 207.
24 D. A. Stuart, A. J. Haes, C. R. Yonzon, E. M. Hicks and R. P. Van Duyne, *IEE Proc.: Nanobiotechnol.*, 2005, **152**, 13.
25 N.-S. Lai, C.-C. Wang, H.-L. Chiang and L.-K. Chau, *Anal. Bioanal. Chem.*, 2007, **388**, 901.
26 C.-Y. Chiang, M.-L. Hsieh, K.-W. Huang, L.-K. Chau, C.-M. Chang and S.-R. Lyu, *Biosens. Bioelectron.*, 2010, **26**, 1036.
27 L.-K. Chau, Y.-F. Lin, S.-F. Cheng and T.-J. Lin, *Sens. Actuators, B*, 2006, **113**, 100.
28 Y. Chuang, C.-Y. Lee, S.-H. Lu, S.-C. Wang, L.-K. Chau and W.-H. Hsieh, *Anal. Chem.*, 2010, **82**, 1123.
29 W.-T. Hsu, W.-H. Hsieh, S.-F. Cheng, C.-P. Jen, C.-C. Wu, C.-H. Li, C.-Y. Lee, W.-Y. Li, L.-K. Chau, C.-Y. Chiang and S.-R. Lyu, *Anal. Chim. Acta*, 2011, **697**, 75.
30 M. D. DeGrandpre and L. W. Burgess, *Anal. Chem.*, 1988, **60**, 2582.
31 R. Ince and R. Narayanaswamy, *Anal. Chim. Acta*, 2006, **569**, 1.
32 A. Kausaite-Minkstimiene, A. Ramanaviciene and A. Ramanavicius, *Analyst*, 2009, **134**, 2051.
33 R. Hao, D. Wang, X. e. Zhang, G. Zuo, H. Wei, R. Yang, Z. Zhang, Z. Cheng, Y. Guo, Z. Cui and Y. Zhou, *Biosens. Bioelectron.*, 2009, **24**, 1330.
34 C. D. Bain, E. B. Troughton, Y.-T. Tao, J. Evall, G. M. Whitesides and R. G. Nuzzo, *J. Am. Chem. Soc.*, 1989, **111**, 321.
35 M.-N. Silvia, S. Jürgen, L. Martha, N. Gabriele, W. Michael, B. Roberta, W. Gerhard and K. Wolfgang, *Biosens. Bioelectron.*, 1995, **10**, 903.
36 T. M. Battaglia, J.-F. Masson, M. R. Sierks, S. P. Beaudoin, J. Rogers, K. N. Foster, G. A. Holloway and K. S. Booksh, *Anal. Chem.*, 2005, **77**, 7016.
37 O. R. Bolduc, J. N. Pelletier and J.-F. o. Masson, *Anal. Chem.*, 2010, **82**, 3699.
38 T.-C. Chang, C.-C. Wu, S.-C. Wang, L.-K. Chau and W.-H. Hsieh, *Anal. Chem.*, 2013, **85**, 245.
39 R. Kurita, Y. Yokota, A. Ueda and O. Niwa, *Anal. Chem.*, 2007, **79**, 9572.
40 S.-R. Lyu, D. S. Liu, C. E. Tseng, H. S. Wang and L. K. Chau, in *Osteoarthritis – Diagnosis, Treatment and Surgery*, ed. Q. Chen, InTech – Open Access Publisher, Rijeka, 2012, ch. 21, pp. 379–404.
41 K. Linnet, *Clin. Chem.*, 1993, **39**, 424.
42 E. Dalaveris, T. Kerenidi, A. Katsabeki-Katsafli, T. Kiropoulos, K. Tanou, K. I. Gourgoulianis and K. Kostikas, *Lung Cancer*, 2009, **64**, 219.
43 V. Gubala, L. F. Harris, A. J. Ricco, M. X. Tan and D. E. Williams, *Anal. Chem.*, 2011, **84**, 487.

